Am J Physiol, Heart Circ Physiol: H-00228-2016-R1

Partial I_{K1} blockade destabilizes spiral wave rotation center without inducing wave breakup and facilitates termination of reentrant arrhythmias in ventricles

Yasunori Kushiyama,[1] Haruo Honjo,[1] Ryoko Niwa,[1]Hiroki Takanari,[1] Masatoshi Yamazaki,[1] Yoshio Takemoto,[1] Ichiro Sakuma,[2] Itsuo Kodama,[1] Kaichiro Kamiya[1]

[1]Department of Cardiovascular Research, Research Institute of Environmental Medicine, Nagoya University, Nagoya Japan
[2]Graduate School of Engineering, The University of Tokyo, Tokyo Japan

Running head: I_{K1} blockade destabilizes spiral wave reentry
No financial conflicts of interest

Address correspondence:
Dr. Haruo Honjo
Department of Cardiovascular Research
Research Institute of Environmental Medicine
Nagoya University
Furo-cho, Chikusa-ku
Nagoya464-8601, Japan
E-mail: honjo@riem.nagoya-u.ac.jp
FAX: +81-52-789-5003

Abbreviations

AP	action potential
$APD_{(90)}$	action potential duration (at 90% repolarization)
BCL	basic cycle length
BDM	2,3-butanedione monoxine
$CV_{(L/T)}$	(longitudinal/transverse) conduction velocity
dV/dt_{max}	maximum action potential upstroke velocity
FBL	functional block line
I_{K1}	inward rectifier K^+ current
LV/RV	left/right ventricle
PS	phase singularity
SW	spiral wave
VT/VF	ventricular tachycardia/fibrillation
$WL_{(L/T)}$	(longitudinal/transverse) wave length

Abstract

It has been reported that blockade of the inward rectifier K^+ current (I_{K1}) facilitates termination of ventricular fibrillation (VF). We hypothesized that partial I_{K1}-blockade destabilizes spiral wave (SW) reentry, leading to its termination. Optical action potential (AP) signals were recorded from left ventricles of Langendorff-perfused rabbit hearts with endocardial cryoablation. The dynamics of SW reentry was analyzed during ventricular tachycardia (VT) induced by cross-field stimulation. Intercellular electrical coupling in the myocardial tissue was evaluated by the space constant. In separate experiments, AP recordings were made using the microelectrode technique from right ventricular papillary muscles of rabbit hearts. Ba^{2+} (10-50 μM) caused a dose-dependent prolongation of VT cycle length and facilitated termination of VT in perfused hearts. Baseline VT was maintained by a stable rotor where a SW rotated around an I-shaped functional block line (FBL). Ba^{2+} at 10 μM prolonged I-shaped FBL and phase singularity (PS) trajectory, while Ba^{2+} at 50 μM transformed the SW rotation dynamics from a stable linear pattern to unstable circular/cycloidal meandering. The SW destabilization was not accompanied by SW breakup. Under constant pacing, Ba^{2+} caused a dose-dependent prolongation of APs, and Ba^{2+} at 50 μM decreased conduction velocity. In papillary muscles, Ba^{2+} at 50 μM depolarized the resting membrane potential. The space constant was increased by 50 μM Ba^{2+}. Partial I_{K1}-blockade destabilizes SW rotation dynamics through a combination of prolongation of the wave length, reduction of excitability and enhancement of electrotonic interactions, which facilitates termination of ventricular tachyarrhythmias.

Key words:

Inward rectifier K^+ current; Spiral wave reentry; Ventricular tachycardia; Optical mapping

Background

Ventricular fibrillation/tachycardia (VF/VT) is a main cause of sudden cardiac death, and spiral wave (SW) reentry, which is also referred to as rotors, is a principal mechanism by which VF/VT is maintained (10, 18, 30). Previous studies have reported that modulation of I_{K1} has profound effects on VF/VT and rotor dynamics in ventricles (4, 22). Warren *et al*. (29) have shown that partial blockade of the inward rectifier K^+ current (I_{K1}) by Ba^{2+} decreases the dominant frequency of excitation and the number of coexisting rotors during VF, facilitating VF termination in Langendorff-perfused guinea pig hearts. Noujaim *et al* (15). have investigated the rotor dynamics in a transgenic mouse model overexpressing Kir2.1 in cardiac-specific manner, and they have demonstrated that transgenic ventricles with I_{K1} upregulation accommodate stable rotors with high rotation frequency, which promotes to sustain long-lasting VF/VT. Mathematical simulations have demonstrated that I_{K1} upregulation shortens the action potential duration (APD) in the vicinity of the unexcited core and improves excitability during reentrant activity, synergy of which allows high-frequency rotors to stabilize (15). In cultured monolayers of neonatal rat ventricular myocytes with regions of Kir2.1 gene modification, stable high-frequency rotors were induced with Kir2.1 overexpression, whereas lower frequency meandering rotors were observed with Kir2.1 dominant-negative suppression (24). These results indicate that I_{K1} plays important roles in stabilizing SW reentry (9, 28).

It is well recognized that I_{K1} has critical roles in determining electrophysiological properties of cardiac myocytes (4, 14). I_{K1} is the major transmembrane ionic current to hold the resting membrane potential (RMP) close to the equilibrium potential of K^+ to control electrical excitability. In addition, I_{K1} facilitates action potential (AP) repolarization predominantly in the terminal phase to influence the length of electrical refractoriness. Besides these actions, I_{K1} is a major factor to regulate electrotonic interactions mediated by the local circuit current between abutting cardiac myocytes, because electrical membrane resistance at the RMP level is mainly determined by theconductance of I_{K1}.

Theoretical considerations suggest that alterations of electrotonic interactions between cardiac myocytes have significant influence on the SW rotation dynamics (11, 12, 27). We have recently demonstrated, in isolated rabbit ventricular myocardium, that a pharmacological increase in gap junctional coupling destabilizes SW rotation, by inducing localized conduction block near the SW rotation center (25, 27). However, the effects of I_{K1} blockade on electrotonic interactions and the dynamics of SW reentry have remained incompletely understood. We hypothesized that partial I_{K1}-blockade destabilizes the SW rotation center and facilitates termination of reentrant activity through mechanisms involving an enhancement of electrotonic interactions combined with prolongation of wavelength (WL) and reduction of membrane excitability. We tested this hypothesis in isolated 2-dimensional rabbit ventricles by high-resolution optical mapping.

Methods

The study conforms to the Guide for the Care and Use of Laboratory Animals, and the protocol was approved by the Institutional Animal Care and Use Committee at Nagoya University.

Optical mapping experiments

The procedures of optical mapping are essentially the same as reported previously (8, 31). In brief, hearts were removed from anesthetized male Japanese white rabbits (2.0-2.4 kg, *n*=37) and perfused on a Langendorff apparatus at 37ºC with KR solution containing (in mM) NaCl 120, KCl 4, $CaCl_2$ 1.2, $MgSO_4$ 1.3, $NaHCO_3$ 25.2, NaH_2PO_4 1.2, glucose 5.8 (equilibrated with 95%O_2-5%CO_2). 2-dimensional ventricular myocardium was prepared by cryoablation of the LV endocardium. Hearts were stained with di-4-ANEPPS and fluorescence images (256×256 pixels) of the LV anterolateral surface were recorded by a high-speed camera at 1,000 frames/s. 2,3-butanedione monoxine (BDM,15 mM) was added to the perfusate to minimize motion artifacts, unless otherwise specified. Time points at 10% depolarization and 90% repolarization were identified from normalized action potential (AP) signals, and their interval was defined as APD at 90% repolarization (APD_{90}). The phase mapping method was applied to analyze the VT dynamics (7). Phase singularity (PS), the organizing rotation center of SW reentry, was identified in each frame of consecutive 1,000 images, and total length of a path along which each PS traveled in a unit of time (PS trajectory length per 1,000 ms) was calculated by numerical integration (27). Distant bipolar electrogram (ECG) was recorded to monitor the ventricular activity. $BaCl_2$ (10-50 μM) was added to the perfusate for 10 min to block I_{K1} partially.

Induction of VT and measurements of electrophysiological property

VT was induced by modified cross-field stimulation (*n*=26): a 20-V monophasic DC shock was applied to ventricles in a direction perpendicular to propagation of basic excitations (S_1) from the LV apex (basic cycle length, BCL, 400 ms) (8, 31). The S_1-DC shock coupling interval was adjusted until sustained VT was induced.

In a separate series of experiments (*n*=6), constant pacing (BCL, 200 ms) was applied to the LV anterior wall, and APD_{90} (average of 16 sites, 18x18 mm) and conduction velocity (CV) in the longitudinal or transverse direction (CV_L or CV_T) were measured during elliptical propagation. Wave length (WL) in the longitudinal or transverse direction (WL_L or WL_T) was estimated by the product of APD_{90} and CV_L or CV_T. Spatial APD heterogeneity was evaluated by the difference between the maximum and minimum APD_{90} values obtained from 16 sites. Data were obtained before and after cumulative application of 10-50 μM Ba^{2+}.

Electrotonic interactions via intercellular coupling were evaluated by the length constant in the myocardial tissue, as described previously (1, 25, 27). In brief, a subthreshold cathodal stimulus was applied through a fine electrode and the exponential decay of electrotonic depolarization in the vicinity (0-2 mm) of the electrode was analyzed to obtain the space constant (n=5). In these experiments, the perfusate K^+ concentration was raised to 6 mM to reduce myocardial excitability.

Isolated tissue microelectrode experiments

APs were recorded under constant pacing (BCL, 1,000 ms) from isolated right ventricular (RV) papillary muscle preparations using conventional microelectrode technique (n=5). The preparations were superfused with KR solution at 32ºC, because electrophysiological properties of superfused preparations are better preserved at this temperature. Data were obtained before and after cumulative application of 10-50 μM Ba^{2+}.

Statistical analyses

Data are presented as means±SEM. Analysis of variance followed by Bonferroni's test was used for multiple comparisons. Comparisons of data from the same and different rabbit were made using Student's paired and unpaired t-test, respectively. P<0.05 was considered statistically significant.

Results

Effect of Ba^{2+} on VT cycle length and sustainability

Sustained VT (lasting>5 min) was induced in Langendorff-perfused hearts by cross-field stimulation and Ba^{2+} (10 or 50 μM) was added to the perfusate for 10 min to block I_{K1} partially. Figure 1 shows the rate of VT termination (Fig. 1A) and average VT cycle length before (baseline), during Ba^{2+} application (Figs. 1B,C). In control hearts without Ba^{2+} application, VT was sustained in all hearts (n=5) and VT cycle length was stable (120-130 ms) up to 20 min after VT induction (n=5). Partial blockade of I_{K1} by 10 μM Ba^{2+} terminated VT in 4 out of 10 hearts and significantly increased VT cycle length from 127±3 ms (n=10) to 160±4 ms (n=6) at 10 min (P<0.05). Application of a higher concentration of Ba^{2+} (50 μM) increased the percentage of VT termination (7 out of 10 hearts) and caused greater prolongation of VT cycle length from 126±4 (n=10) to 182±7 ms (n=3) at 10 min (P<0.05). After Ba^{2+} was washed out, VT cycle length returned toward the baseline level before Ba^{2+} application. VT cycle length immediately before VT termination during 10 or 50 μM Ba^{2+} exposure (189±6 ms, n=11) was significantly longer than VT cycle length at 10 min after Ba^{2+} application in hearts in which VT was sustained (VT sustained, 167±5 ms, n=9, P<0.05, Fig. 1C).

SW dynamics at baseline and after 10 µM Ba^{2+} application

Figure 2 demonstrates the dynamics of SW reentry underlying sustained VT at baseline (A-C) and after exposure to 10 µM Ba^{2+} (D-F). At baseline, ECG showed a monomorphic VT pattern with cycle length of 134 ms (Fig. 2A, *top*). Isochronal activation maps during VT (beat *a*) demonstrates a SW rotating clockwise around a short I-shaped line of functional block (FBL, Fig. 2B, *left*), and this pattern repeated (Fig. 2A, *bottom*). The phase mapping method was applied to analyze the SW dynamics. A phase singularity (PS) moved back and forth along a short straight line (Fig. 2B, *right*), which corresponds to the FBL. The stable SW rotation pattern was maintained during the VT episode (Fig. 2C).

After application of 10 µM Ba^{2+}, VT cycle length was increased to 152 ms and finally VT terminated (Fig. 2D, *top*). The length of the I-shaped FBL and corresponding PS trajectory (beat *b*) was increased compared to the baseline (Fig. 2E, b). Conduction block occurred in the reentry circuit (beat *c*), which is shown by the PS moving toward the LV base (Fig. 2E, c, *right*). Subsequently the PS collided with the atrioventricular groove, resulting in termination of the reentrant activity (Fig. 2E, c, *right*). The PS trajectory plotted on time-space axes illustrates PS destabilization and annihilation by collision with the anatomical boundary (Fig. 2F).

SW dynamics after 50 µM Ba^{2+} application

Figure 3 shows SW reentry after application of 50 µM Ba^{2+} in another heart. In this heart, stable SW rotation around a short FBL was maintained before Ba^{2+} application (Suppl. Movie 1). SW reentry during exposure to 50 µM Ba^{2+} was complex (Suppl. Movie 2). Figures 3B and 3C show isochronal activation maps and phase maps of three consecutive beats (beats *a*-*c* in Fig. 3A), 8 min after Ba^{2+} application. In beat *a*, a SW rotated clockwise around a prolonged I-shaped FBL (Fig. 3B, a), which is also illustrated by a long PS trajectory line in the phase map (Fig. 3C, a). In beat *b*, AP signals shows conduction block around the center of SW rotation (site 4), resulting in the formation of an additional FBL. The phase map shows that a PS moved toward the LV base along the new FBL. In addition, conduction block caused a dramatic change in the FBL in the subsequent beat *c*. A sequence of SW rotation composed of these three patterns (*a*-*c*) exhibits unstable circular/cycloidal meandering (Fig. 3D) and this pattern repeated during the VT episode. Figure 3E shows the SW dynamics immediately before VT termination. The SW rotation pattern in beat *d* was similar to that in beat *b*, and conduction block occurred in beat *e* in the isthmus between the FBL and the atrioventricular groove, leading to VT termination. A time-space plot of PS trajectory exhibits circular/cycloidal PS meandering, followed by PS annihilation by collision with the anatomical boundary at the atrioventricular groove (Fig. 3F).

Effects of Ba^{2+} on SW dynamics

The effects of partial I_{K1} blockade by 10 or 50 μM Ba^{2+} on SW reentry were investigated in a total of 20 hearts (10 hearts for each concentration, Fig. 4). Representative PS dynamics in 6 hearts are shown in Fig. 4A. At baseline, PS trajectory exhibited a short line in all 20 hearts. After exposure to 10 μM Ba^{2+}, the PS trajectory was prolonged but still remained linear in all 10 hearts tested. The axis of PS trajectory was irrespective of myocardial fiber orientation before and after 10 μM $BaCl_2$ application. The length of PS trajectory by numerical integration for 1,000 ms was significantly increased (from 8.1±0.9 cm to 12.3±1.7 cm, n=10, P<0.05, Fig. 4B). The PS trajectory length was measured either immediately before VT termination or at 10 min after Ba^{2+} application in hearts in which VT was sustained. After exposure to 50 μM Ba^{2+}, PS trajectory was transformed from a linear pattern to unstable circular/cycloidal meandering in 5 out of 10 hearts, and PS trajectory was greatly prolonged (from 7.9±1.0 cm to 16.1±2.3 cm, n=10, P<0.05, Fig. 4B). The average length of PS trajectory during exposure to 50 μM Ba^{2+} (16.1 cm, average of 10 hearts) was longer than that during exposure to 10 μM Ba^{2+}, (12.3 cm, average of other 10 hearts), although the difference was statistically insignificant (P=0.21, unpaired t-test). It is important to note that such destabilization of SW rotation dynamics was not accompanied by an increase in the number of SWs. The number of PS remained nearly one in the presence of Ba^{2+}, indicating that the well-organized excitation pattern was maintained even after destabilization of SW rotation center (Fig. 4C).

The length of FBL during SW reentry was also quantified before and after $BaCl_2$ application. When two successive isochrones of 4-ms intervals were superimposed at a single pixel (local CV<~3 cm/s), local conduction block was defined at that site (8). FBL immediately before SW termination during 10 or 50 μM Ba^{2+} exposure was significantly longer (17.5±1.0 mm, n=11) than FBL during SW that was sustained after Ba^{2+} application (9.6±1.4 mm, n=9, P<0.05, Fig. 4D). There was a weak positive correlation between VT cycle length and FBL length during 10 or 50 μM Ba^{2+} exposure (r=0.45, P=0.045, n=20, Fig. 4E).

Essentially the same results were obtained with application of 50 μM Ba^{2+} in a heart untreated with BDM, although large motion artefacts hampered detailed analysis of the excitation dynamics (data not shown).

Effects of Ba^{2+} on electrophysiological properties under constant pacing

I_{K1} plays pivotal roles in the maintenance of the stable resting membrane potential (RMP) and contributes to AP repolarization. We assessed the effects of Ba^{2+} on APs and CV under constant pacing (BCL, 200 ms). Elliptical propagation of excitations emanating from a stimulation point was optically mapped before and during Ba^{2+} exposure. Ba^{2+} (10-50 μM) caused a dose-dependent prolongation of APD_{90} (from 130±2 ms to 148±2 ms at 10 μM Ba^{2+}, 164±3 ms at 50 μM Ba^{2+}, n=6, P<0.05, Fig. 5A). While Ba^{2+} at 10 μM caused no significant change in CV_L and CV_T, Ba^{2+} at 50 μM significantly decreased CV_L (from 54.0±0.9 cm/s to

49.0±0.6 cm/s, n=6, P<0.05) and CV_T (from 22.5±0.4 cm/s to 19.4±0.3 cm/s, n=6, P<0.05, Fig. 5B). WL was estimated by the product of APD_{90} and CV. Ba^{2+} at 10 and 50 μM significantly prolonged WL_L and WL_T compared to the baseline values before Ba^{2+} application (Fig. 5C). There was no significant difference in spatial APD heterogeneity before (15.8±2.6 ms) and after application of 50 μM Ba^{2+} (15.0±1.8 ms, n=6, P=0.77).

Because the absolute membrane potential cannot be obtained by optical mapping, we performed additional microelectrode experiments in isolated RV papillary muscles. Representative APs (BCL, 1,000 ms) before and after exposure to Ba^{2+} are shown in Fig. 6A. Consistent with the results from Langendorff-perfused hearts, Ba^{2+} (10-50 μM) caused a dose-dependent APD prolongation in ventricular papillary muscles (Fig. 6B). While Ba^{2+} at 10 μM caused no significant change in RMP and maximum AP upstroke velocity (dV/dt_{max}), Ba^{2+} at 50 μM significantly depolarized RMP (from -81.3±1.4 mV to -77.1±2.1 mV, n=5, P<0.05, Fig. 6C) and decreased dV/dt_{max} (from 153±19 V/s to 127±12 V/s, n=5, P<0.05, Fig. 6D), again consistent with the Ba^{2+}-induced CV changes in optical mapping experiments.

Effects of Ba^{2+} on the space constant

I_{K1} is a major determinant in regulation of the membrane resistance at the RMP level, and changes in the membrane resistance theoretically affect intercellular electrical interactions. We measured the space constant before and after Ba^{2+} application (Fig. 7). The space constant is proportional to the square root of the ratio of membrane resistance/tissue resistance, and membrane resistance at the RMP level is mainly determined by the conductance of I_{K1}. Ba^{2+} at 50 μM significantly increased the space constant (from 0.8±0.1 mm to 1.1±0.1 mm in the transverse direction, n=5, P<0.05), suggesting that partial I_{K1} blockade enhances electrotonic influence from the surrounding myocardium.

Discussion

The key observations from this study are summarized as follows. 1) Partial I_{K1} blockade by Ba^{2+} increased VT cycle length and facilitated termination of sustained VT. 2) Weak I_{K1} blockade (by 10 μM Ba^{2+}) prolonged FBL and corresponding PS trajectory during VT, while stronger I_{K1} blockade (by 50 μM Ba^{2+}) transformed the type of SW rotation dynamics from a linear pattern to unstable circular/cycloidal meandering, which was not associated with SW breakup. 3) Under constant pacing, weak I_{K1} blockade prolonged APD without affecting RMP, whereas stronger I_{K1} blockade caused RMP depolarization accompanied by reduction of dV/dt_{max} and CV, in addition to APD prolongation. 4) I_{K1} blockade increased the space constant in the ventricular tissue.

Mechanisms of SW destabilization and VT termination by I_{K1} blockade

In a thin layer of ventricular myocardium, stable rotation of SW reentry around a short FBL was maintained during sustained VT, and partial I_{K1} blockade by 10-50 μM Ba^{2+} facilitated termination of SW reentry. The VT termination rate increased with raising the Ba^{2+} concentration (from 40% at 10 μM to 70% at 50 μM), which was associated with changes in the SW dynamics. The linear pattern of SW rotation was preserved with weak I_{K1} blockade by 10 μM Ba^{2+}, although the length of FBLs was increased. In contrast, stronger I_{K1} blockade by 50 μM Ba^{2+} destabilized the SW rotation dynamics, resulting in its transformation from stable linear pattern to unstable circular/cycloidal meandering.

The prolongation of linear FBLs by weak I_{K1} blockade may reflect prolongation of APD and consequent increase in WL (11, 12, 19). Under constant pacing, 10 μM Ba^{2+} caused prolongation of APD and increase in WL without significant changes in other electrophysiological parameters. When the prolonged FBL reached to an unexcitable anatomical boundary, the reentrant activity terminated.

On the other hand, the SW destabilization by stronger I_{K1} blockade may be mediated by multiple electrophysiological factors (4, 9, 18, 28). Theoretical studies have demonstrated that the type of SW rotation depends on the level of excitability and the length of refractoriness (11, 12, 19). In the cardiac tissue with high excitability and considerable refractory period, the SW tip moves along its own refractory tail, which serves a FBL, and at the end of the FBL, the wave tip makes a turn. With reducing excitability, interactions between the wavefront and the refractory tail at the SW tip become weaker but fluctuate, resulting in the loss of rotation stability to form unstable cycloidal meandering. When excitability is further reduced, propagation of the wavefront is not affected by the wave tail, and the SW tip follows a circular trajectory, because the tip cannot extend toward the rotation center due to curvature-dependent source-sink mismatch of the local excitatory current. In the present study, 50 μM Ba^{2+} caused decreases in dV/dt_{max} and CV associated with RMP depolarization under constant pacing, indicating that excitability of the ventricular tissue is reduced by 50 μM Ba^{2+}. In addition, 50 μM Ba^{2+} significantly increased the WL. The expansion of refractory tissue enhances wavefront-to-tail interactions at the SW tip, which may also contribute to the SW destabilization. Moreover, the SW dynamics is known to be affected by the influence of the unexcited core (9, 18, 28). Previous studies have reported that I_{K1} overexpression in a transgenic mouse model enhances electrotonic currents between unexcited cells in the core and active cells in its immediate vicinity and this reduces CV very close to the core, which helps establish a fast and stable rotor (15). The higher concentration of Ba^{2+} (50 μM) in this study potentially increases Ca^{2+} currents and this effect would be expected to enhance SW destabilization by providing additional depolarizing currents.

Alterations of electrotonic interactions have significant influence on SW rotation (11, 12, 27). Propagation of excitation waves in the hearts is affected by the geometry of the excitation wave front: when the wave front is convex, propagation velocity is reduced compared with

that of a flat wave front (curvature effect). The curvature effect is modulated by alterations of electrical coupling between cardiac myocytes (11, 12, 27). We have previously demonstrated that a pharmacological increase in gap junctional coupling enhances the curvature effect on excitation wave propagation and destabilizes SW rotation dynamics by inducing localized conduction block near the rotation center, where the SW front is strongly curved (25, 27). In the present study, partial I_{K1} block by 50 μM Ba^{2+} increased the space constant by 37%, indicating that electrotonic interactions between cardiac myocytes is enhanced. The diastolic membrane potential around the pivot point of SW reentry is expected to be depolarized compared with that in the spiral arm distant from the pivot point. It is possible that elevated diastolic potential would increase the space constant and thus exacerbate the curvature effect, which facilitates destabilization of SW rotation. The experimental data of the present and our previous studies (27) suggest that modification of electrotonic interactions have significant influence on excitation wave propagation around the pivot point of SW reentry, and then the FBL of SW reentry should be sensitive to the propagation direction in myocardium with anisotropy. The experimental data, however, showed that partial I_{K1} block by 10 μM Ba^{2+} extended the FBL almost equally in both transverse and longitudinal directions in viable 2-dimensional epicardial myocardium. The present optical mapping experiments cannot provide data to explain its underlying mechanisms and further studies including mathematical simulations are require. Finally, it is possible that alterations of electrotonic interactions affect the SW dynamics through a modification of spatial heterogeneity of AP repolarization. The optical mapping data, however, show that there was no significant difference in spatial APD heterogeneity during constant pacing before and after 50 μM Ba^{2+} application, suggesting that the contribution of this mechanism to Ba^{2+}-induced modification of SW dynamics may be minimal under experimental conditions in the present study..

Clinical implications

The present study demonstrates that partial I_{K1} blockade by Ba^{2+} facilitates termination of SW reentry by destabilizing the SW rotation dynamics in ventricular myocardium. Most of class III antiarrhythmic drugs (K^+ channel blockers) currently available prolongs the refractory period mainly blocking the rapid component of the delayed rectifier K^+ current (I_{Kr}). We have previously shown that nifekalant, a selective I_{Kr} blocker, produces SW destabilization leading to its early termination (31). There is a remarkable difference in modification of functional reentry by Ba^{2+} predominantly blocking late phase 3/terminal repolarization (I_{K1} blockade) and that by nifekalant prolonging the AP plateau and blocking early repolarization (I_{Kr} blockade). The SW destabilization by nifekalant was associated with frequent SW breakup at the spiral arm away from its tip, resulting in the formation of new rotors. In contrast, the present study demonstrates that I_{K1} blockade by Ba^{2+} destabilized the SW rotation center inducing linear or cycloidal/circular meandering without enhancing

instability in the spiral arm that causes SW breakup. This is particularly important from a clinical point of view, suggesting that appropriate I_{K1} blockade facilitates VT termination with much less risk of degeneration into multiple-wavelet type VF as compared with currently available I_{Kr} blockers.

It must be mentioned that excessive I_{K1} blockade is at risk of ventricular proarrhythmia by the focal mechanisms, such as depolarization-induced automaticity and triggered activity (14). Warren *et al* (29) have documented very slow polymorphic VT in isolated guinea pig hearts after VF termination by application of 50 μM Ba^{2+}. In addition, ventricular tachyarrhythmia is one of the classic triad of Andersen-Tawil syndrome that is associated with a loss-of-function mutation in the Kir2.1 channel subunit gene (*KCNJ2*) (20). A recent simulation study, however, has shown that a gain-of-function mutation in *KCNJ2* found in short QT syndrome type-3 patients increases vulnerability to ventricular reentry (3).

Pharmacological therapy for prevention of VF, which is targeted toward specific ionic currents, has proved unsatisfactory. Chloroquine is a widely-used antimalarial drug and is shown to be effective in suppression of ventricular and atrial tachyarrhythmias (6, 16, 17). Electrophysiological and molecular structure studies have revealed that chloroquine's antiarrhythmic actions are primarily attributed to its ability to block I_{K1} in cardiomyocytes (16, 17). Recent researches have been focused on the development of new chemical compounds that selectively block I_{K1} (26), and one of pentamidine analogues is reported to have highly I_{K1}-specific blocking potency without affecting other channel function and protein trafficking (23). Nevertheless, I_{K1}-specific blockade may not be an ideal pharmacological antiarrhythmic approach because of the risk of proarrhythmia.

Study limitations

In the present study, Ba^{2+} was added to the perfusate at low concentrations (10-50 μM) to block I_{K1}, because Ba^{2+} is a strong blocker of I_{K1} ($K_{ir}2$ channels) with a 50%-inhibitory concentration (IC_{50}) of ~1-20 μM (13, 14). Ba^{2+} at higher concentrations is known to block other K^+ currents (IC_{50}>100 μM), including the acetylcholine-activated K^+ current ($K_{ir}3$ channels) (2) and two-pore domain K^+ channels (K_{2P} channels) (5), although their contribution to electrophysiological properties of rabbit ventricular muscle is considered to be minimal.

I_{K1} has major roles in determining the RMP not only in cardiac myocytes but also in fibroblasts, which are electrically coupled by gap junctions (21). The I_{K1} blockade-induced SW modification observed in the present study might be attributed in part to changes in the electrical load produced by coupling with fibroblasts. Experiments with cardiomyocyte-specific gene modification technology and/or mathematical simulations are required to evaluate this possibility.

Optical mapping experiments were performed in a thin layer of ventricular myocardium of isolated rabbit hearts, predominantly in the presence of an excitation-contraction decoupling agent. Careful attention must be payed to extrapolate the results of this study to intact human hearts which beat physiologically.

Conclusion

This study demonstrates that partial I_{K1}-blockade destabilizes SW reentry without inducing wave breakup through the synergy of prolongation of the wave length, reduction of excitability and enhancement of electrotonic interactions, which facilitates termination of reentrant ventricular arrhythmias. These results provide important insights into the dynamics of SW reentry and its control by interventions.

Grant

This study was financially supported by MEXT Japan/JSPS Grant-in-Aid for Scientific Research on Innovative Areas 22136010 and Grant-in-Aid for Scientific Research 15K09078.

Disclosures

No conflicts of interest, financial or otherwise, are declared by the author (s)

Author contributions

Author contributions: Y.K., R.N., H.T. and Y.T. performed experiments; Y.K., R.N., H.T. and I.S. analyzed data; Y.K., H.H., H.T. and M.Y. interpreted results of experiments; Y.K. and R.N. prepared figures; Y.K. drafted manuscript; Y.K., H.H. and M.Y. edited and revised manuscript; H.H., I.K. and K.K. conception and design of research; H.H. approved final version of manuscript.

References

1. **Akar FG**, **Roth BJ**, **Rosenbaum DS**. Optical measurement of cell-to-cell coupling in intact heart using subthreshold electrical stimulation. *Am J Physiol Heart Circ Physiol* 281: H533–42, 2001.
2. **Carmeliet E**, **Mubagwa K**. Characterization of the acetylcholine-induced potassium current in rabbit cardiac Purkinje fibres. *J Physiol* 371: 219–37, 1986.
3. **Deo M**, **Ruan Y**, **Pandit S V**, **Shah K**, **Berenfeld O**, **Blaufox A**, **Cerrone M**, **Noujaim SF**, **Denegri M**, **Jalife J**, **Priori SG**. KCNJ2 mutation in short QT syndrome 3 results in atrial fibrillation and ventricular proarrhythmia. *Proc Natl Acad Sci U S A* 110: 4291–6, 2013.
4. **Dhamoon AS**, **Jalife J**. The inward rectifier current (I_{K1}) controls cardiac excitability and is involved in arrhythmogenesis. *Heart Rhythm* 2: 316–324, 2005.
5. **Enyedi P**, **Czirják G**. Molecular background of leak K^+ currents: two-pore domain potassium channels. *Physiol Rev* 90: 559–605, 2010.
6. **Filgueiras-Rama D**, **Martins RP**, **Mironov S**, **Yamazaki M**, **Calvo CJ**, **Ennis SR**, **Bandaru K**, **Noujaim SF**, **Kalifa J**, **Berenfeld O**, **Jalife J**. Chloroquine terminates stretch-induced atrial fibrillation more effectively than flecainide in the sheep heart. *Circ Arrhythm Electrophysiol* 5: 561–70, 2012.
7. **Gray RA**, **Pertsov AM**, **Jalife J**. Spatial and temporal organization during cardiac fibrillation *Nature* 392: 75–8, 1998.
8. **Ishiguro YS**, **Honjo H**, **Opthof T**, **Okuno Y**, **Nakagawa H**, **Yamazaki M**, **Harada M**, **Takanari H**, **Suzuki T**, **Morishima M**, **Sakuma I**, **Kamiya K**, **Kodama I**. Early termination of spiral wave reentry by combined blockade of Na^+ and L-type Ca^{2+} currents in a perfused two-dimensional epicardial layer of rabbit ventricular myocardium. *Heart Rhythm* 6: 684–692, 2009.
9. **Jalife J**. Inward rectifier potassium channels control rotor frequency in ventricular fibrillation. *Heart Rhythm* 6: S44–8, 2009.
10. **Jalife J**. Ventricular fibrillation: mechanisms of initiation and maintenance. *Annu Rev Physiol* 62: 25–50, 2000.
11. **Kléber AG**, **Janse MJ**, **Fast VG**. Normal and abnormal conduction in the heart. In *Handbook of Physiology. Oxford: Oxford University Press*; 2001:455-530.
12. **Kléber AG**, **Rudy Y**. Basic mechanisms of cardiac impulse propagation and associated arrhythmias. *Physiol Rev* 84: 431–88, 2004.
13. **Liu GX**, **Derst C**, **Schlichthörl G**, **Heinen S**, **Seebohm G**, **Brüggemann A**, **Kummer W**, **Veh RW**, **Daut J**, **Preisig-Müller R**. Comparison of cloned Kir2 channels with native inward rectifier K^+ channels from guinea-pig cardiomyocytes. *J Physiol* 532: 115–26, 2001.

14. **Lopatin AN**, **Anumonwo JMB**. Structure and basis of cardiac inward rectifier potassium channel function. In: *Cardiac Electrophysiology from Cell to Bedside, 6th edition,* edited by Zipes DP, Jalife J, Philadelphia: Saunders: 2014:33-41.
15. **Noujaim SF**, **Pandit SV**, **Berenfeld O**, **Vikstrom K**, **Cerrone M**, **Mironov S**, **Zugermayr M**, **Lopatin AN**, **Jalife J**. Up-regulation of the inward rectifier K+ current (I_{K1}) in the mouse heart accelerates and stabilizes rotors. *J Physiol* 578: 315–326, 2007.
16. **Noujaim SF**, **Stuckey JA**, **Ponce-Balbuena D**, **Ferrer-Villada T**, **López-Izquierdo A**, **Pandit S**, **Calvo CJ**, **Grzeda KR**, **Berenfeld O**, **Sánchez-Chapula JA**, **Jalife J**. Specific residues of the cytoplasmic domains of cardiac inward rectifier potassium channels are effective antifibrillatory targets. *FASEB J* 24: 4302–4312, 2010.
17. **Noujaim SF**, **Stuckey JA**, **Ponce-Balbuena D**, **Ferrer-Villada T**, **López-Izquierdo A**, **Pandit S V**, **Sánchez-Chapula JA**, **Jalife J**. Structural bases for the different anti-fibrillatory effects of chloroquine and quinidine. *Cardiovasc Res* 89: 862–9, 2011.
18. **Pandit SV**, **Jalife J**. Rotors and the dynamics of cardiac fibrillation. *Circ Res* 112: 849–62, 2013.
19. **Panfilov AV**. Theory of reentry. In: *Cardiac Electrophysiology from Cell to Bedside, 5th edition,* edited by Zipes DP, Jalife J, Philadelphia: Saunders; 2009:329-337.
20. **Plaster NM**, **Tawil R**, **Tristani-Firouzi M**, **Canún S**, **Bendahhou S**, **Tsunoda A**, **Donaldson MR**, **Iannaccone ST**, **Brunt E**, **Barohn R**, **Clark J**, **Deymeer F**, **George AL**, **Fish F a.**, **Hahn A**, **Nitu A**, **Ozdemir C**, **Serdaroglu P**, **Subramony SH**, **Wolfe G**, **Fu YH**, **Ptáček LJ**. Mutations in Kir2.1 cause the developmental and episodic electrical phenotypes of Andersen's syndrome. *Cell* 105: 511–519, 2001.
21. **Qi X-Y**, **Huang H**, **Ordog B**, **Luo X**, **Naud P**, **Sun Y**, **Wu C-T**, **Dawson K**, **Tadevosyan A**, **Chen Y**, **Harada M**, **Dobrev D**, **Nattel S**. Fibroblast inward-rectifier potassium current upregulation in profibrillatory atrial remodeling. *Circ Res* 116: 836–45, 2015.
22. **Samie FH**, **Berenfeld O**, **Anumonwo J**, **Mironov SF**, **Udassi S**, **Beaumont J**, **Taffet S**, **Pertsov a M**, **Jalife J**. Rectification of the background potassium current: a determinant of rotor dynamics in ventricular fibrillation. *Circ Res* 89: 1216–1223, 2001.
23. **Sánchesz-Chapula JA**, **van der Heyden MAG**. Molecular regulation of cardiac inward rectifier potassium channels by pharmacological agents. In: *Cardiac Electrophysiology from Cell to Bedside, 6th edition,* edited by Zipes DP, Jalife J, Philadelphia: Saunders 2014:129-137.
24. **Sekar RB**, **Kizana E**, **Cho HC**, **Molitoris JM**, **Hesketh GG**, **Eaton BP**, **Marbán E**, **Tung L**. I_{K1} heterogeneity affects genesis and stability of spiral waves in cardiac myocyte monolayers. *Circ Res* 104: 355–364, 2009.
25. **Takanari H**, **Honjo H**, **Takemoto Y**, **Suzuki T**, **Kato S**, **Harada M**, **Okuno Y**, **Ashihara T**, **Opthof T**, **Sakuma I**, **Kamiya K**, **Kodama I**. Bepridil facilitates early termination of spiral-wave reentry in two-dimensional cardiac muscle through an increase

of intercellular electrical coupling. *J Pharmacol Sci* 115: 15–26, 2011.

26. **Takanari H**, **Nalos L**, **Stary-Weinzinger A**, **de Git KCG**, **Varkevisser R**, **Linder T**, **Houtman MJC**, **Peschar M**, **de Boer TP**, **Tidwell RR**, **Rook MB**, **Vos MA**, **van der Heyden MAG**. Efficient and specific cardiac I_{K1} inhibition by a new pentamidine analogue. *Cardiovasc Res* 99: 203–214, 2013.
27. **Takemoto Y**, **Takanari H**, **Honjo H**, **Ueda N**, **Harada M**, **Kato S**, **Yamazaki M**, **Sakuma I**, **Opthof T**, **Kodama I**, **Kamiya K**. Inhibition of intercellular coupling stabilizes spiral-wave reentry, whereas enhancement of the coupling destabilizes the reentry in favor of early termination. *Am J Physiol Heart Circ Physiol* 303: H578–H586, 2012.
28. **Vaquero M**, **Calvo D**, **Jalife J**. Cardiac fibrillation: From ion channels to rotors in the human heart. *Heart Rhythm* 5: 872–879, 2008.
29. **Warren M**, **Guha PK**, **Berenfeld O**, **Zaitsev A**, **Anumonwo JMB**, **Dhamoon AS**, **Bagwe S**, **Taffet SM**, **Jalife J**. Blockade of the inward rectifying potassium current terminates ventricular fibrillation in the guinea pig heart. *J Cardiovasc Electrophysiol* 14: 621–631, 2003.
30. **Weiss JN**, **Qu Z**, **Chen PS**, **Lin SF**, **Karagueuzian HS**, **Hayashi H**, **Garfinkel A**, **Karma A**. The dynamics of cardiac fibrillation. *Circulation* 112: 1232–1240, 2005.
31. **Yamazaki M**, **Honjo H**, **Nakagawa H**, **Ishiguro YS**, **Okuno Y**, **Amino M**, **Sakuma I**, **Kamiya K**, **Kodama I**. Mechanisms of destabilization and early termination of spiral wave reentry in the ventricle by a class III antiarrhythmic agent, nifekalant. *Am J Physiol Heart Circ Physiol* 292: H539–H548, 2007.

Figure legends

Figure 1. VT termination and changes in VT cycle length in response to Ba^{2+} application. Sustained VT (lasting >5 min) was induced in Langendorff-perfused hearts and $BaCl_2$ (10 or 50 μM) was added to the perfusate for 10 min (*n*=10 for each concentration). **A.** VT was sustained in 5/5 hearts without Ba^{2+} application (control), whereas VT was terminated in 4/10 and 7/10 hearts during exposure to 10 and 50 μM Ba^{2+}, respectively. **B.** VT cycle length before (baseline) and after Ba^{2+} application (10 or 50 μM, *n*=10 for each concentration). **C**. Comparison of VT cycle length immediately before VT termination (*n*=9) during Ba^{2+} exposure and VT cycle length at 10 min after Ba^{2+} application in hearts in which VT was sustained (*n*=11). $^{*}P<0.05$ vs. baseline, $^{+}P<0.05$ vs. VT sustain.

Figure 2. Spiral wave (SW) dynamics at baseline (A-C) and after 10 μM Ba^{2+} application (D-F). **A.** Representative electrocardiacgram (ECG) and optical action potential (AP) tracings during sustained VT at baseline. **B.** An isochronal activation map (*left*) of beat *a* in panel **A** and corresponding trajectory of phase singularity (PS, black line) drawn on a phase map (*right*). **C.** PS trajectory at baseline plotted on time-space axes. **D.** ECG and optical AP tracings after 10 μM Ba^{2+} application. **E**. Isochronal activation maps and PS trajectory of beats *b* (*top*) and *c* (*bottom*) in panel **D**. **F.** A time-space plot of PS trajectory during VT after 10 μM Ba^{2+} application. Yellow lines in isochronal maps show FBLs and white circles in phase maps indicate PSs.

Figure 3. Spiral wave (SW) dynamics after 50 μM Ba^{2+} application. A. ECG (*top*) and optical action potential (AP) tracings (*bottom*) during VT after application of 50 μM Ba^{2+}. **B, C.** Isochronal activation maps (**B**) and trajectory of phase singularity (PS) drawn on phase maps (**C**) of 3 consecutive beats (*a-c* in panel **A**). **D**. superimposed PS trajectory during these 3 beats (*a-c*). **E**. Isochronal activation maps of the last 2 beats immediately before VT termination (*d* and *e* in panel **A**). **F.** A time-space plot of PS trajectory during VT after 50 μM Ba^{2+}. Yellow lines and pink broken arrows in isochronal maps show FBLs and conduction block, respectively. White circles in phase maps indicate PSs.

Figure 4. Effects of Ba^{2+} on spiral wave (SW) dynamics. **A.** Representative PS trajectory during sustained VT at baseline and after application of 10 μM Ba^{2+} in 3 hearts (*top*) or 50 μM Ba^{2+} in other 3 hearts (*bottom*). **B.** Average length of phase singularity (PS) trajectory per unit of time (1,000 ms) at baseline and after application of 10 or 50 μM Ba^{2+}. **C.** Average number of PS detected in the observation area during sustained VT at baseline and after 10 or 50 μM Ba^{2+} application. $^{*}P<0.05$ vs. baseline. **D.** Comparison of functional block line (FBL) length of SW reentry immediately before VT termination (*n*=9) during exposure to Ba^{2+} and FBL length at 10 min after Ba^{2+} application in hearts in which VT was sustained (*n*=11).

$^{+}P<0.05$ vs. VT sustain. **E.** Correlation between VT cycle length and FBL length during exposure to 10 and 50 μM Ba^{2+} (n=20). In this analysis, VT cycle length and FBL length were measured either immediately before VT termination or at 10 min after Ba^{2+} application in hearts in which VT was sustained.

Figure 5. Effects of Ba^{2+} on electrophysiological properties in ventricles of Langendorff-perfused hearts under constant pacing. A-C. Action potential duration at 90% repolarization ($APD_{90,}$ average of 16 sites, **A**), longitudinal and transverse conduction velocity (CV_L and CV_T, respectively, **B**) and wave length (WL_L and WL_T, respectively, **C**) under constant pacing (basic cycle length, 200 ms) at baseline and after application of 10 and 50 μM Ba^{2+}. WL was estimated by the product of APD_{90} and CV. $^{*}P<0.05$ vs. baseline, $^{+}P<0.05$ vs. baseline and 10 μM Ba^{2+}.

Figure 6. Effects of Ba^{2+} on action potetnials of papillary muscles. A. Representative action potentials and their first derivatives (*inset*) recorded from right ventricular papillary muscles under constant pacing (basic cycle length, 1,000 ms) at baseline and after application of 10 and 50 μM Ba^{2+}. **B-D.** Action potential duration at 90% repolarization (APD_{90}, **B**), resting membrane potential (RMP, **C**) and maximum action potential upstroke velocity ($dV/dt_{max,}$ **D**) at baseline and after application of 10 and 50 μM Ba^{2+}. Data were obtained at 32 ºC. $^{*}P<0.05$ vs. baseline, $^{+}P<0.05$ vs. baseline and 10 μM Ba^{2+}.

Figure 7. Effects of Ba^{2+} on electrotonic interactions. A, B. The space constant was measured to evaluate electrotonic interactions in ventricles of Langendorff-perfused hearts. A subthrethold cathodal stimulus (S_2) was applied through a fine electrode following a sprathreshold stimulus (S_1), and the decay of electrotonic subthreshold depolarization in the vicinity of the stimulation site was fitted by a single exponential function to obtain the space constant (*arrows* in **B**). **C.** The space constant in the transverse direction at baseline and after application of 50 μM Ba^{2+}. $^{*}P<0.05$ vs. baseline.

Supplemental Materials

Supplement Movie 1. SW reentry dynamics at baseline (voltage map movie).

Supplement Movie 2. SW reentry dynamics after 50 μM Ba^{2+} application (voltage map movie).

Figure 1

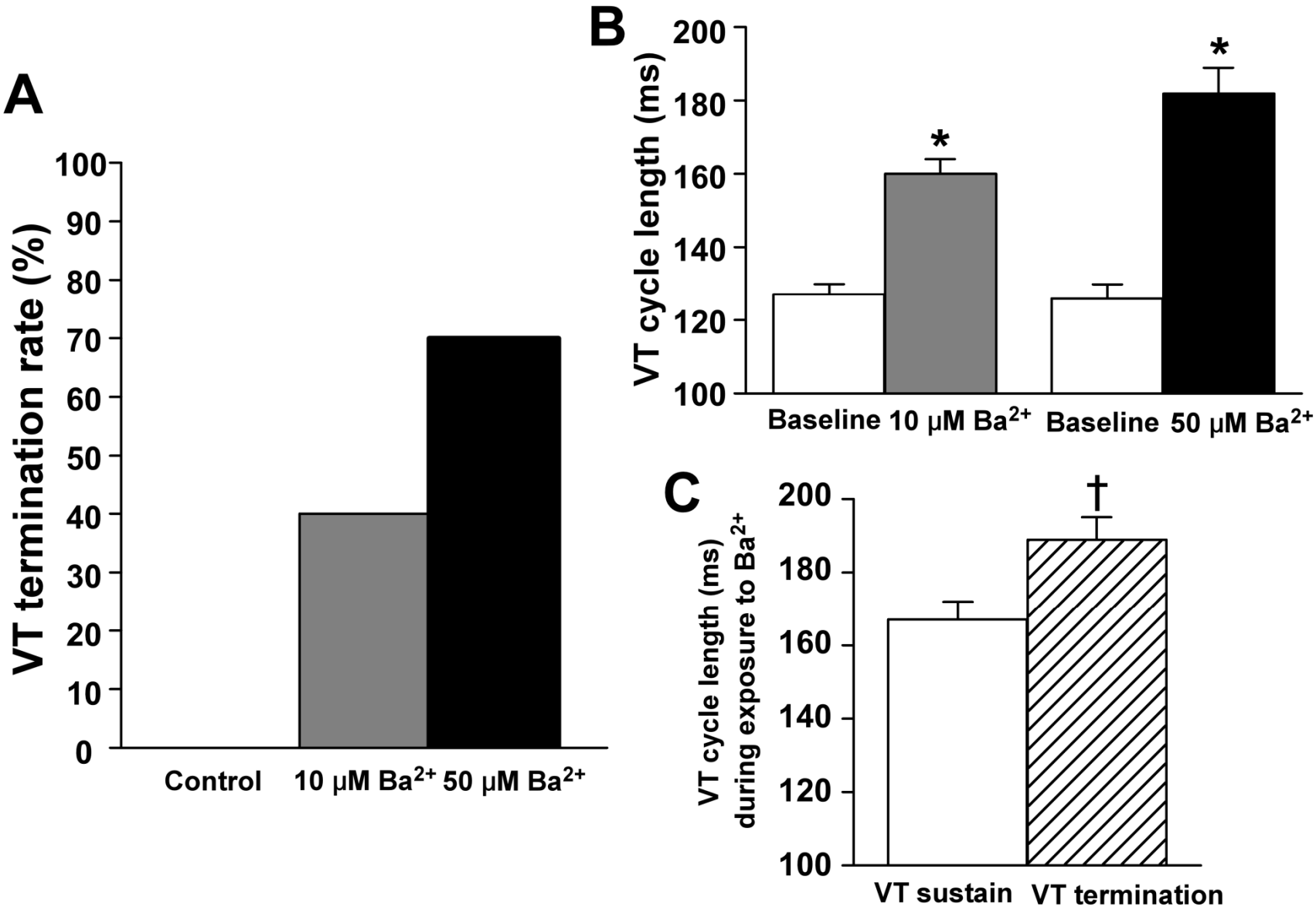
A
VT termination rate (%)
100
90
80
70
60
50
40
30
20
10
0
Control
10 μM Ba2+
50 μM Ba2+
B
VT cycle length (ms)
200
180
160
140
120
100
*
*
Baseline
10 μM Ba2+
Baseline
50 μM Ba2+
C
VT cycle length (ms) during exposure to Ba2+
200
180
160
140
120
100
†
VT sustain
VT termination

Figure 2

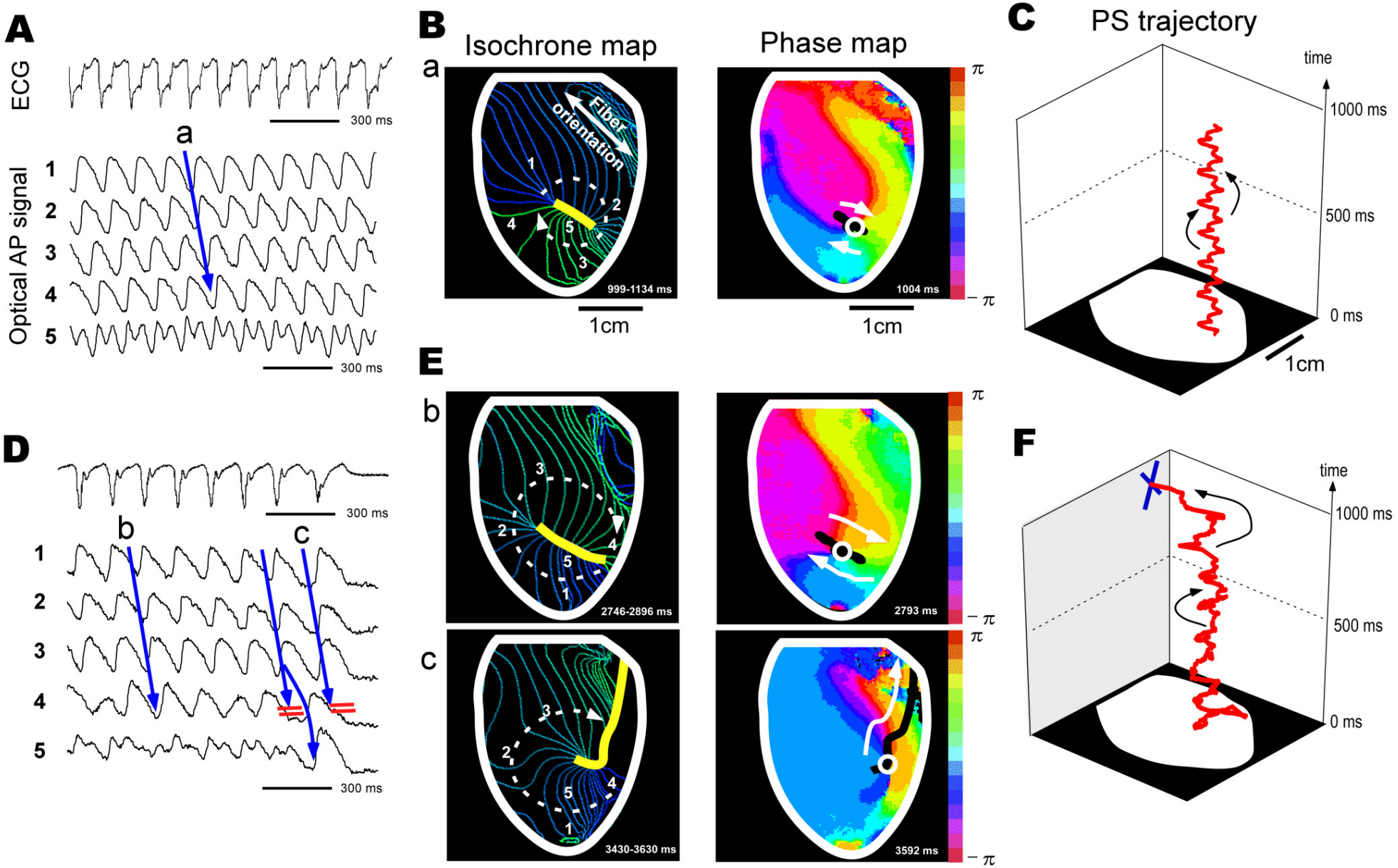
A
ECG
300 ms
a
Optical AP signal
1
2
3
4
5
300 ms
D
300 ms
b
c
1
2
3
4
5
300 ms
B
Isochrone map
Phase map
a
Fiber orientation
1
2
3
4
5
999-1134 ms
1cm
1004 ms
1cm
π
– π
E
b
2746-2896 ms
2793 ms
c
3430-3630 ms
3592 ms
C
PS trajectory
time
1000 ms
500 ms
0 ms
1cm
F
time
1000 ms
500 ms
0 ms

Figure 3

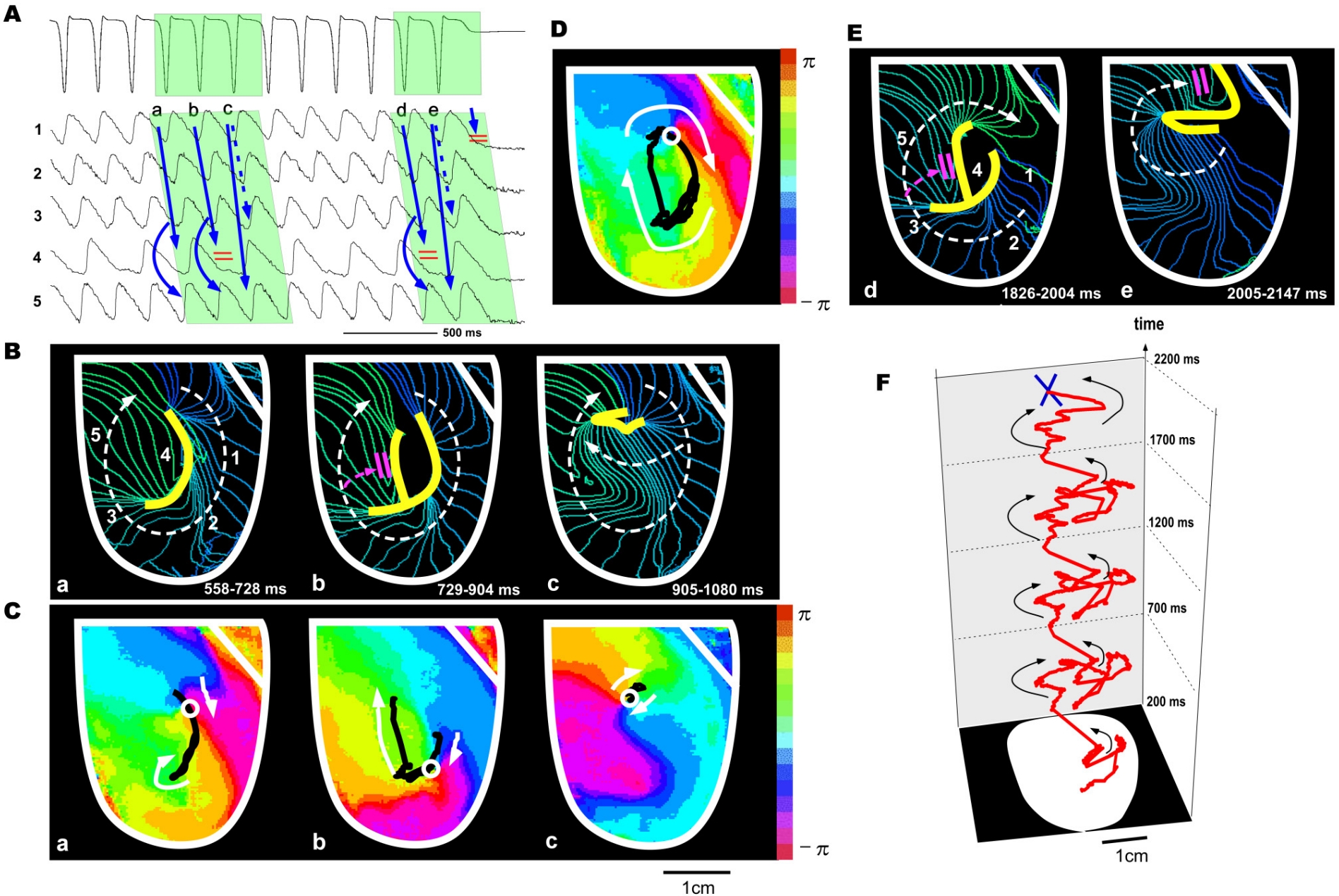
A
a b c d e
1
2
3
4
5
500 ms
D
π
− π
E
5
4
1
3
2
d
1826-2004 ms
e
2005-2147 ms
time
B
5
4
1
3
2
a
558-728 ms
b
729-904 ms
c
905-1080 ms
C
π
− π
a
b
c
1cm
F
2200 ms
1700 ms
1200 ms
700 ms
200 ms
1cm

Figure 4

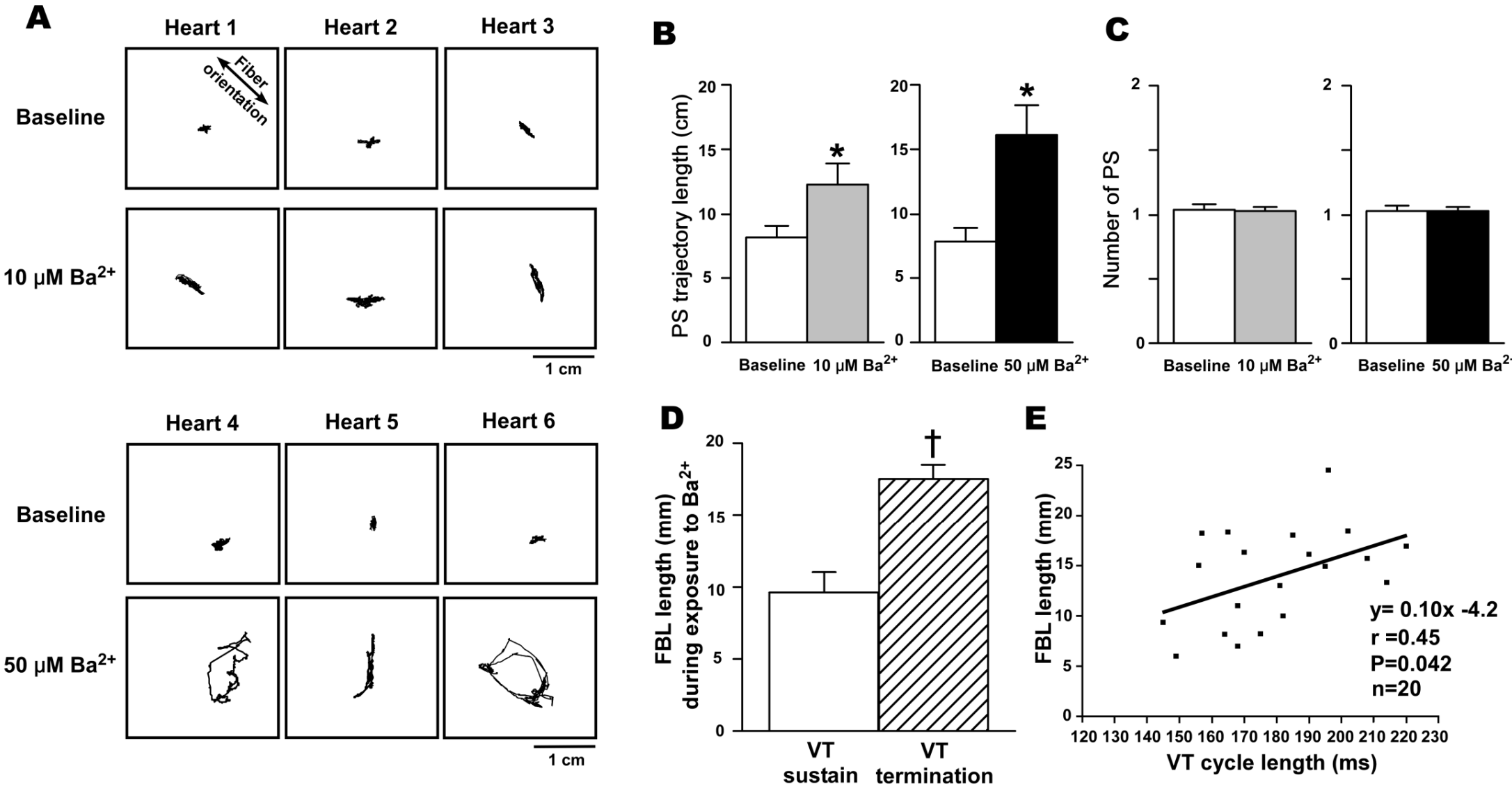
A
Heart 1
Heart 2
Heart 3
Fiber orientation
Baseline
10 μM Ba2+
1 cm
Heart 4
Heart 5
Heart 6
Baseline
50 μM Ba2+
1 cm
B
PS trajectory length (cm)
Baseline 10 μM Ba2+
Baseline 50 μM Ba2+
C
Number of PS
Baseline 10 μM Ba2+
Baseline 50 μM Ba2+
D
FBL length (mm) during exposure to Ba2+
VT sustain
VT termination
E
FBL length (mm)
VT cycle length (ms)
y= 0.10x -4.2
r =0.45
P=0.042
n=20

Figure 5

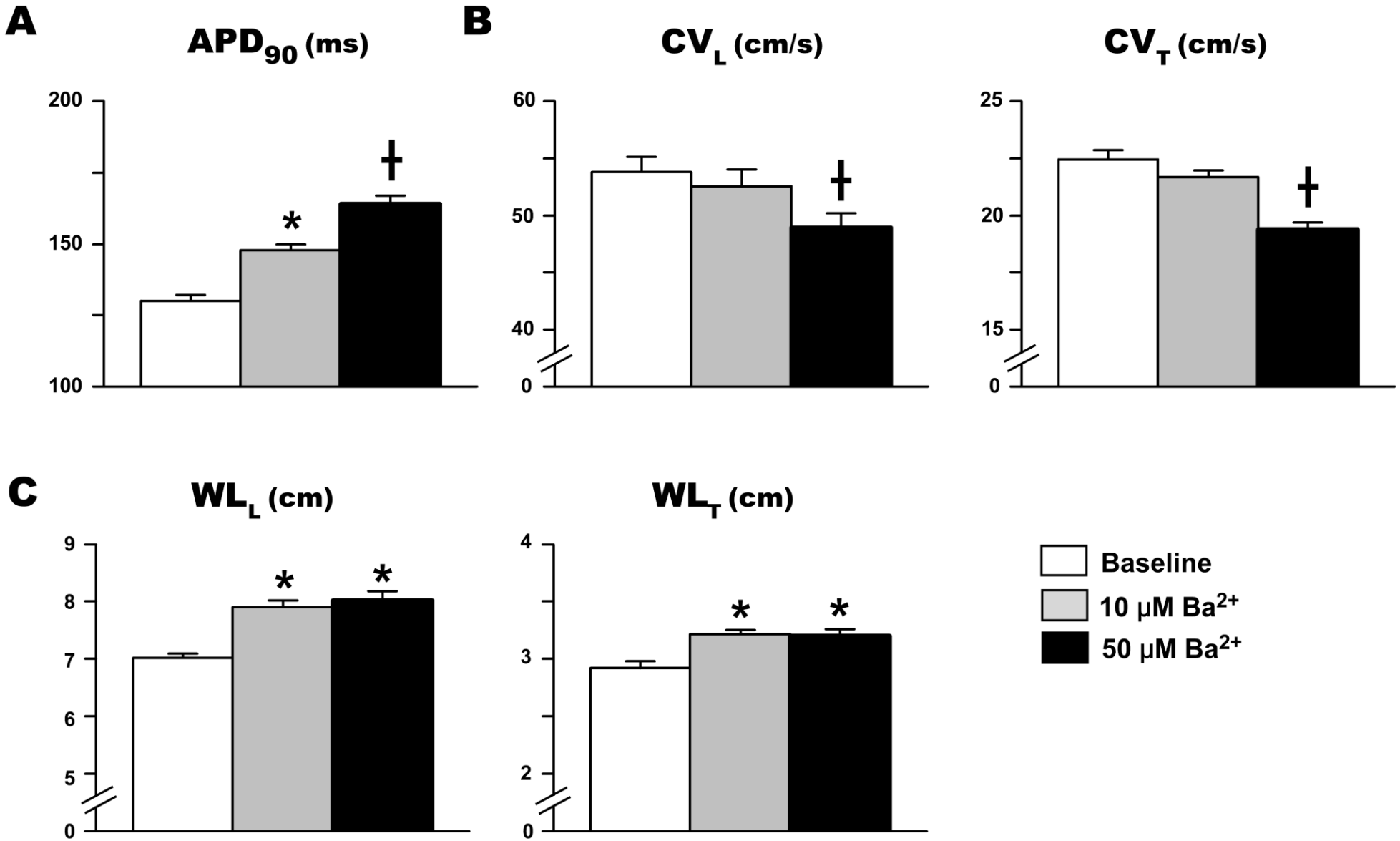
A
APD90 (ms)
200
150
100
*
†
B
CVL (cm/s)
60
50
40
0
†
CVT (cm/s)
25
20
15
0
†
C
WLL (cm)
9
8
7
6
5
0
*
*
WLT (cm)
4
3
2
0
*
*
Baseline
10 μM Ba2+
50 μM Ba2+

Figure 6

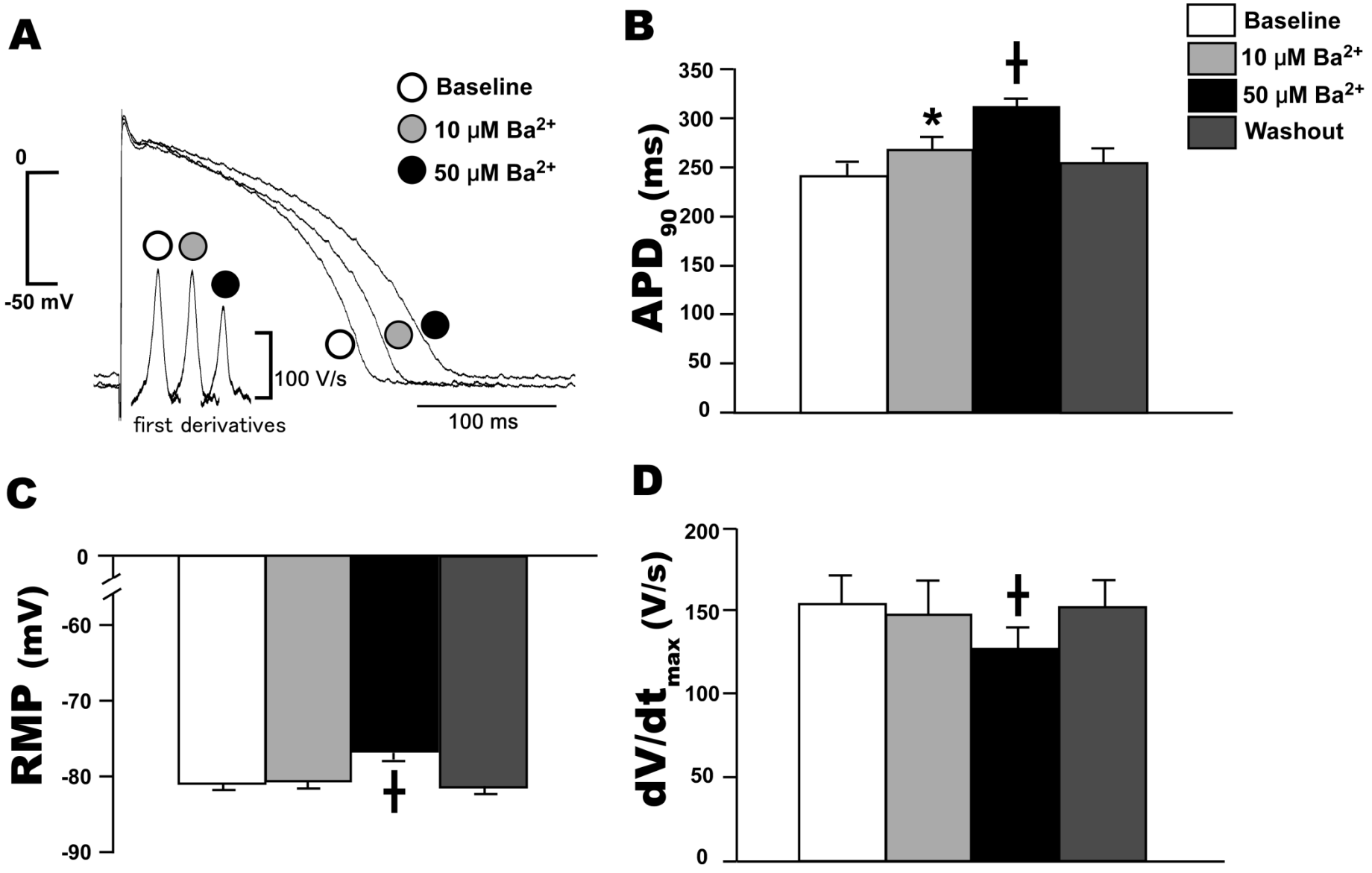
A
Baseline
10 μM Ba2+
50 μM Ba2+
0
-50 mV
100 V/s
first derivatives
100 ms
B
Baseline
10 μM Ba2+
50 μM Ba2+
Washout
APD90 (ms)
350
300
250
200
150
100
50
0
*
†
C
RMP (mV)
0
-60
-70
-80
-90
†
D
dV/dtmax (V/s)
200
150
100
50
0
†

Figure 7

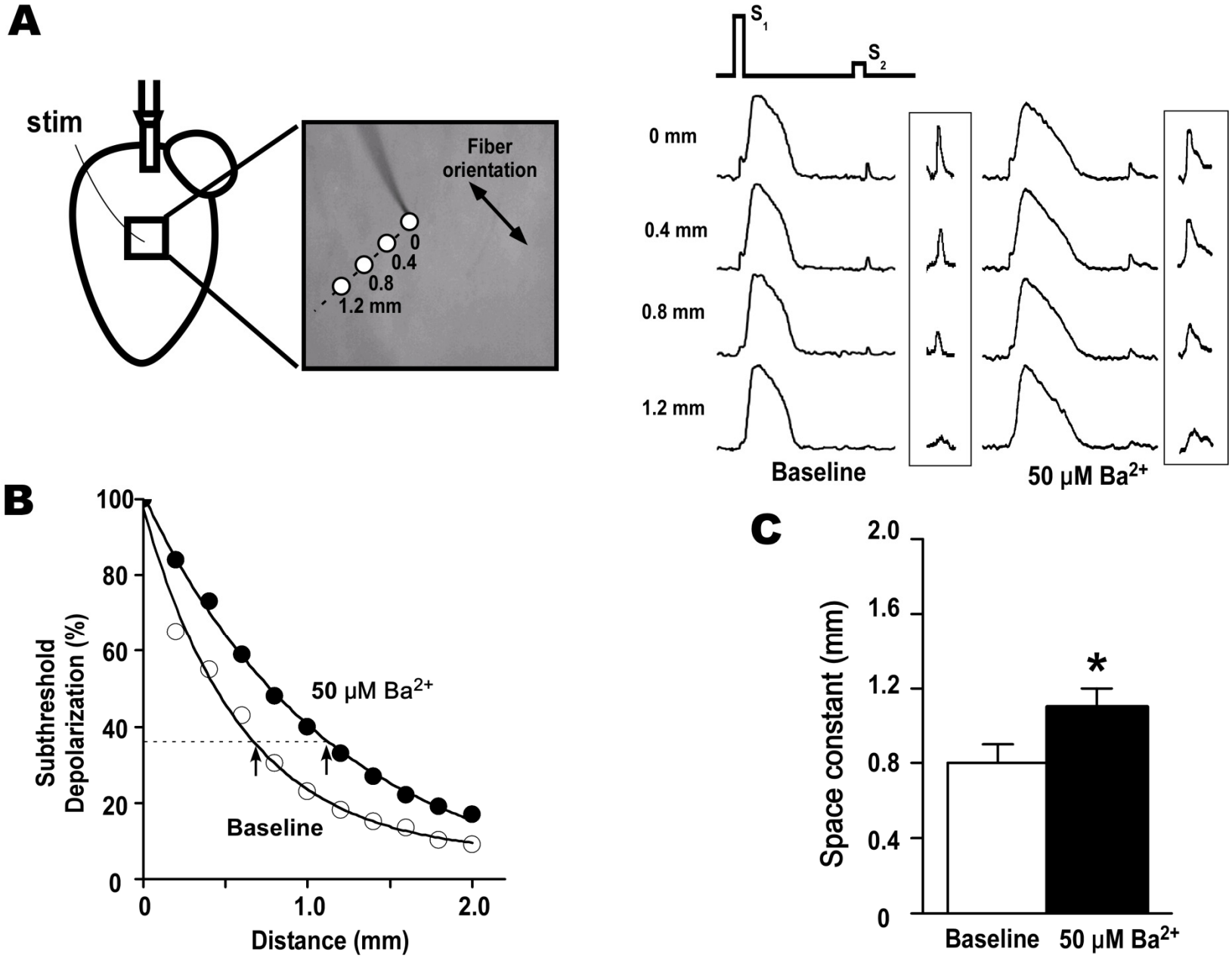
A
stim
Fiber orientation
0
0.4
0.8
1.2 mm
S1
S2
0 mm
0.4 mm
0.8 mm
1.2 mm
Baseline
50 µM Ba2+
B
Subthreshold Depolarization (%)
100
80
60
40
20
0
50 µM Ba2+
Baseline
0
1.0
2.0
Distance (mm)
C
Space constant (mm)
2.0
1.6
1.2
0.8
0.4
0
*
Baseline
50 µM Ba2+